Energy Technology
Generation, Conversion, Storage, Distribution
www.entechnol.de

The New Material Battery Based on Mg/C-π

Rikson Siburian, Suriati Paiman, Fajar Hutagalung, Ab Malik Marwan Ali, Lisnawaty Simatupang, and Crystina Simanjuntak*

Herein, the effect of the size of Mg clusters on graphene nano sheets (GNS) and N-GNS (C-π) is investigated. The dependence of the electric conductivities of C-π on the electrolytes was also explored. This work aims to clarify the size effect of Mg clusters on Mg/C-π and to study the effect of addition of electrolytes to C-π materials on their electrical conductivities and chemical interaction between Mg on GNS and N-GNS, respectively. GNS and N-GNS are synthesized by modified Hummers and N-dopant method at room temperature, respectively. Characterization of each material is carried out using X-ray diffraction (XRD), scanning electron microscope–energy dispersive X-ray (SEM–EDX), and multimeter. The results show that the Mg cluster are well deposited on GNS and N-GNS and the addition of Mg metal and electrolyte materials can increase the electrical conductivities of Mg/GNS (69.9301 $\mu S\ cm^{-1}$) and Mg/N-GNS (96.1538 $\mu S\ cm^{-1}$), comparing to graphite (26.7 $\mu S\ cm^{-1}$) and anode of commercial battery (26.0 $\mu S\ cm^{-1}$). The addition of electrolyte can also increase the reduction power of Mg metal particles and the electron mobility of Mg/GNS and Mg/N-GNS materials. Interestingly, the electrolyte could reduce the size of Mg clusters and modulate the mobility of electrons. Data conclude that Mg/GNS and Mg/N-GNS can be produced into battery electrodes with better electrical conductivity.

1. Introduction

The rapid advancement of technology in the modern era has led to an increase in battery requirements.[1] Batteries are electrochemical devices that are able to convert chemical energy into electrical energy and can store electrical energy in the form of chemical energy through electrochemical reactions, which involve the transfer of electrons from between other materials through an electrical circuit.[2] Ideal batteries should have high specific energy and power density,[3,4] low cost,[5] resistance to interference,[6] and good life cycle.[7,8]

One of the most widely used battery types today is the Li-ion battery.[9] This battery became popular because it has various advantages such as specific capacity (100–180 $Ah\ kg^{-1}$),[10] no memory effect,[11] and environmental-friendly property, because the power reduction process is slow when not in use,[12] energy can be increased by the charge–discharge process,[13] gravimetric density in electrical equipment applications (94 $Wh\ kg^{-1}$) is higher than Ni–Cd batteries (35 $Wh\ kg^{-1}$) and Ni–MH (47 $Wh\ kg^{-1}$),[14] specific power (300 $W\ kg^{-1}$),[15] and a relatively long life cycle (≈1000 cycles).[16] The LiB-based electrode material provides an advantage in its use because Li has a standard potential (−3.05 V vs the standard hydrogen electrode), has the lowest atomic mass (6.94 $g\ mol^{-1}$, $\rho = 0.53\ g\ cm^{-3}$) of all metals,[17] and has the third smallest radius (145 pm) compared with other single charged ions so that it is able to diffuse ionically well.[18] Li (alkali metal) is able to remove its valence electrons easily and act as a graphene N-doping agent, so that it can form strong ionic bonds (with Li–graphene spacing as 0.25 nm) to modify the magnetic and electronic properties of graphene.[19,20] The atomic charges of Li and Li^+ in the Li/graphene alloy are +0.654 and +0.721, respectively, indicating that Li has dual properties, namely, as an electron donor and acceptor on the graphene surface.[21,22] However, until now, there are still various problems in the development of Li-based LiB electrode materials, namely, 1) the expensive price of Li raw material (≈$6000/ton) and[23] the decreasing availability of lithium metal in nature[24] and 2) Li, as a chemically reactive metal with its anode surface, shows dendritic growth at high current densities, which can cause internal short circuits and serious safety issues and can damage performance and reduce battery life.[25]

R. Siburian, F. Hutagalung, C. Simanjuntak
Chemistry Department
Universitas Sumatera Utara
Medan 20155, Indonesia
E-mail: rikson@usu.ac.id

R. Siburian, C. Simanjuntak
Carbon Research Center
Universitas Sumatera Utara
Medan 20155, Indonesia

S. Paiman
Physics Department, Faculty of Science
Universiti Putra Malaysia
43400 (Serdang) Seri Kembangan, Selangor, Malaysia

A. M. M. Ali
Faculty of Applied Sciences
Universiti Teknologi MARA
Shah Alam 40450, Selangor, Malaysia

L. Simatupang
Department of Chemistry, Faculty of Mathematics and Natural Sciences
Universitas Negeri Medan
Jl. Willem Iskandar Psr. V, Medan 20221, Indonesia

The ORCID identification number(s) for the author(s) of this article can be found under https://doi.org/10.1002/ente.202100453.

DOI: 10.1002/ente.202100453

Graphene has a large surface area[26] and has π-orbitals[27] so that it can interact with metal nanoparticles,[28] and deposition of metal into the graphene structure with the aim of inhibiting and reducing the possibility of agglomeration between graphene sheets (nanospacer agents) so as to increase the active surface area,[29] electronic conductivity, and the ionic diffusion potential of graphene occurs.[30] Magnesium (Mg) has good thermal and electrical conductivity, low equivalent weight and density (1.74 g cm^{-3}),[23] a low potential (–2.38 V), a hexagonal structure, is not easy to slip when interacting with other elements, nontoxic,[31] abundant (about 2.3% by weight of the Earth's crust) and widespread, cheap (≈$1000/ton), and has a fairly high charge storage capacity (2205 mAh g^{-1} vs 3862 mAh g^{-1} for Li) and theoretical volumetric capacity (3833 mAh cm^{-3} vs 2046 mAh cm^{-3} for Li).[32] The Mg/graphene alloy shows physical adsorption characters because there is almost no charge transfer from Mg to graphene.[33] The atomic charge of Mg (–0.201) and Mg^{+} (+0.555) ion on graphene shows that Mg and Mg^{+} act as electron acceptors on the surface of graphene (Mg–graphene distance is 0.2019 nm).[34] Mg and graphene alloys used as battery electrodes show outstanding performance. Previous research has been conducted by Malyala (2019), which uses graphene and magnesium on battery electrode.[29] The cyclic voltammetry analysis of Mg/graphene alloys shows good reversibility (specific capacity 55 mAh g^{-1} and average discharge voltage −1.15 V) at constant current (0.1 mA cm^{-2}) and good life cycle (80 cycles), which indicates a stable discharge capacity and good electrochemical properties.

Additives such as electrolytes can be used to improve the performance of the battery electrodes.[35] This was explained by Li (2014), who reported that the interaction between the graphene electrode and the electrolyte could improve the electrochemical performance of the electrode. Electrolyte acts as an ion-transfer medium, so it is able to produce battery electrodes with a higher conductivity value than before, being combined with the electrolyte material. Ion activity in electrolyte paste is a charge transport process in the battery system, which is caused by diffusion and migration and electrochemical reactions that take place on the surface between the electrodes and electrolytes. The simulation results show that the presence of electrolyte at the electrodes can affect the conductivity of the battery.[36]

This research was conducted to determine the size effect of Mg metal and the addition of electrolytes on graphene nanosheets (GNS) and N-graphene nanosheets (N-GNS) materials, and the electrical conductivity and chemical interaction between Mg and GNS and N-GNS are expected to produce battery electrodes with better electrical conductivity.

2. Results

2.1. Mg/GNS and Mg/N-GNS Preparation

In this study, the precursor $MgCl_2.6H_2O$ was used as a source of Mg metal, which is expected to be deposited in the GNS and N-GNS structures. The variations in the concentrations of the Mg precursor used were 1, 2, 3, 4, 5, and 10 mg L^{-1}, wherein the concentration (wt%) of each Mg metal that is expected to be deposited theoretically is shown in **Figure 1**. From Figure 1, it can be explained that the use of variations in the concentrations of precursors (in ppm) used increases, indicating that the mass of crystals also increases. This is why the concentration of Mg that is expected to be deposited in both GNS and N-GNS structures also increases. The value of Mg concentration (wt%) is theoretically obtained by comparing the masses of GNS, N-GNS, Mg/GNS, and Mg/N-GNS powders obtained by weighing their respective masses and calculating the percentage of metal concentration of Mg (in wt%) (**Table 1**).

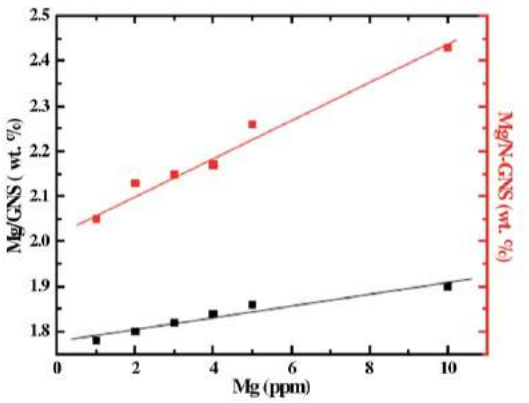

Figure 1. Relation between concentration of Mg precursor (ppm) and the concentration of Mg/GNS (wt%) and Mg/N-GNS (wt%) calculated.

2.2. X-Ray Diffraction (XRD) Analysis

The physical properties of graphitic carbon (graphite, GNS, and N-GNS), Mg/GNS, and Mg/N-GNS were examined by XRD analysis (JCPDS 75–2078). **Figure 2**a shows a sharp and narrow peak at $2\theta = 26.5°$, which is a typical C (002) peak of graphite with the

Table 1. Comparison of the theoretical calculation of the mass percentage concentration (wt%) of Mg deposited with the concentration of the precursor Mg used.

Materials	Mg/GNS mass powder obtained [g]	Calculated Mg deposited [g]	Mg [wt%] (Calculated)
Mg 1 ppm/GNS	0.5876	0.0876	1.78
Mg 2 ppm/GNS	0.5889	0.0889	1.80
Mg 3 ppm/GNS	0.5898	0.0898	1.82
Mg 4 ppm/GNS	0.5910	0.0910	1.84
Mg 5 ppm/GNS	0.5926	0.0926	1.86
Mg 10 ppm/GNS	0.5950	0.0950	1.90
Mg 1 ppm/N-GNS	0.6088	0.1038	2.05
Mg 2 ppm/N-GNS	0.6087	0.1087	2.13
Mg 3 ppm/N-GNS	0.6101	0.1101	2.15
Mg 4 ppm/N-GNS	0.6112	0.1112	2.17
Mg 5 ppm/N-GNS	0.6170	0.1170	2.26
Mg 10 ppm/N-GNS	0.6281	0.1281	2.43

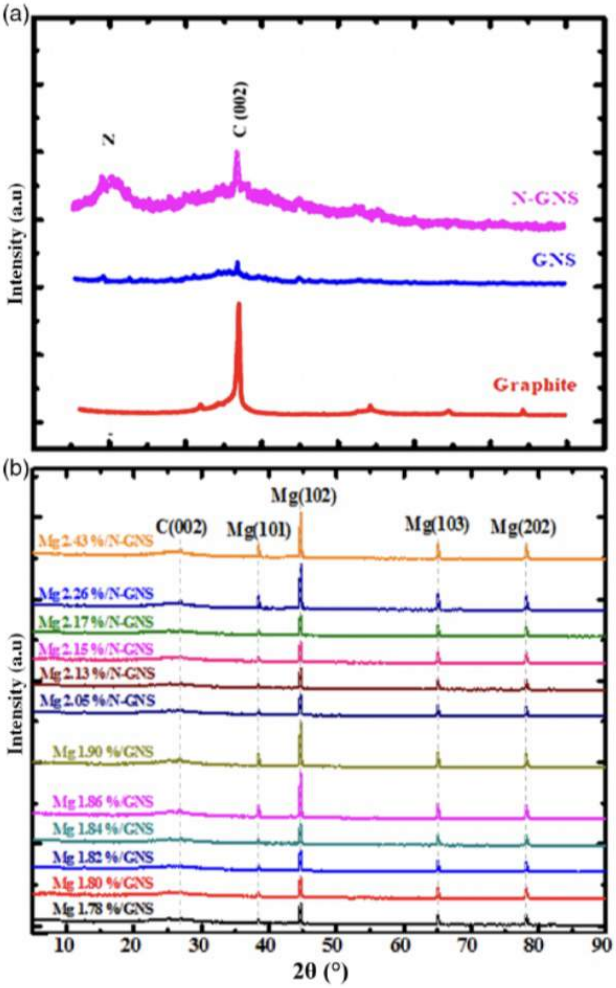

Figure 2. a) XRD patterns of graphite, GNS, N-GNS and b) Mg/GNS with various concentrations of Mg and Mg/N-GNS with various concentrations of Mg.

distance between planars as 3.33 Å.[37] A weak and widening peak at $2\theta = 26.5°$ with d-spacing of 3.35 Å indicates that GNS is formed successfully. The change in the peak of the GNS diffractogram is due to the bonding of oxidized graphite and the entry of oxygen into the graphite interlayer space.[38] N-GNS shows a rather sharp and wide peak at $2\theta = 26.5°$ (d-spacing = 3.39 Å). The doping process of heteroatom (N) from ammonia into the graphene structure will cause site defects and damage in the carbon lattice, which in turn will cause N-graphene to have low crystallinity and cause a small shift in the 2θ value.[39]

2.3. Scanning Electron Microscope–Energy Dispersive X-Ray (SEM–EDX) Analysis

SEM−EDX aims to obtain a view of the later sample surface computed with software to analyze the material components from both quantitative and qualitative aspects of graphitic carbon (graphite, GNS, and N-GNS), Mg/GNS, and Mg/N-GNS. SEM data show that graphite consists of stacked graphene sheets, which are very dense and not uniform (**Figure 3**a). Graphene was synthesized based on graphite as well as a raw material using the modified Hummers' method.[40,41] There is a significant difference between graphite and graphene (SEM data).

In this research, EDX was used to determine the atomic abundance (wt%) in Mg/ GNS and Mg/N-GNS samples, including Mg atoms deposited in the GNS and N-GNS structures. The spectrum obtained is a characteristic of the X-rays captured by the Si detector (**Figure 4**a-l). From the results obtained, the detected Mg particles indicated that Mg atoms were successfully deposited onto the GNS and N-GNS surfaces. The concentration (wt%) with different values of the Mg atom shows the effect of using different precursor concentrations.

Furthermore, the calculation of Mg particles was carried out to explain the average size and size of the Mg particles that were successfully deposited on the GNS and N-GNS surfaces. The particle size histograms (Figure 4a–l) show that Mg particle size at Mg concentrations from 1.78 to 1.80 wt%/GNS decreased and then increased significantly at Mg 1.82 wt%/GNS, decreased significantly at Mg 1.84 wt%/GNS, and then gradually increased back to 1.90% Mg/GNS. Mg 1.82 wt%/GNS has the highest particle size (0.481 μm) and Mg 1.84 wt%/GNS has the smallest particle size (0.337 μm). Mg particle size for Mg concentration 2.05−2.15 wt%/N-GNS increased slowly and then decreased at Mg 2.17–2.26 wt%/N-GNS and increased slowly at Mg 2.43 wt%/N-GNS. Based on Figure 4, Mg 2.15 wt%/N-GNS has the highest particle size (0.495 μm) and Mg 2.26% has the smallest particle size (0.353 μm). The formation of these particles is influenced by size of the metal, density, charge, and shape of the deposited metal particles (**Figure 5**).

2.4. Electrical Conductivity Measurement

This analysis aims to study the effect of NaCl electrolyte paste, in each powder sample material, on their electrical conductivity at room temperature. The value of electrical conductivity is obtained from the calculations

$$\sigma = \frac{1}{R} \tag{1}$$

$$R = \frac{V}{I} \tag{2}$$

where σ = electrical conductivity (μS cm^{-1}); R = electrical resistance (Ohm); V = voltage used (volts), and I = current obtained from the measurement with a multimeter (μA).

Figure 6 shows the relation of voltage versus current and voltage versus electrical conductivity (σ) of graphite, GNS, and N-GNS. The results of the electrical conductivity of N-GNS (51.7 μS cm^{-1}) and GNS (45.4 μS cm^{-1}) show a higher value than graphite (8.5 μS cm^{-1}) because N-GNS and GNS have a higher surface area and thermal conductivity than graphite. In addition, the presence of nitrogen doping into the graphene structure (C−N interaction and electron transfer from nitrogen to graphene atoms) is able to increase the surface area of graphene and open the energy gap between the conductance band and the valence band of graphene, thereby increasing electron mobility and electrical conductivity. The electrical conductivity of graphite increases at a voltage of 20 V and then begins to decline

Mg/N-GNS (wt%) showed that different Mg particle sizes were deposited at Mg/GNS[42] and Mg/N-GNS.[43] The weak and broad peaks for Mg (102) indicate that the Mg particles size is small. Thereby, we may modify the properties of Mg with surface

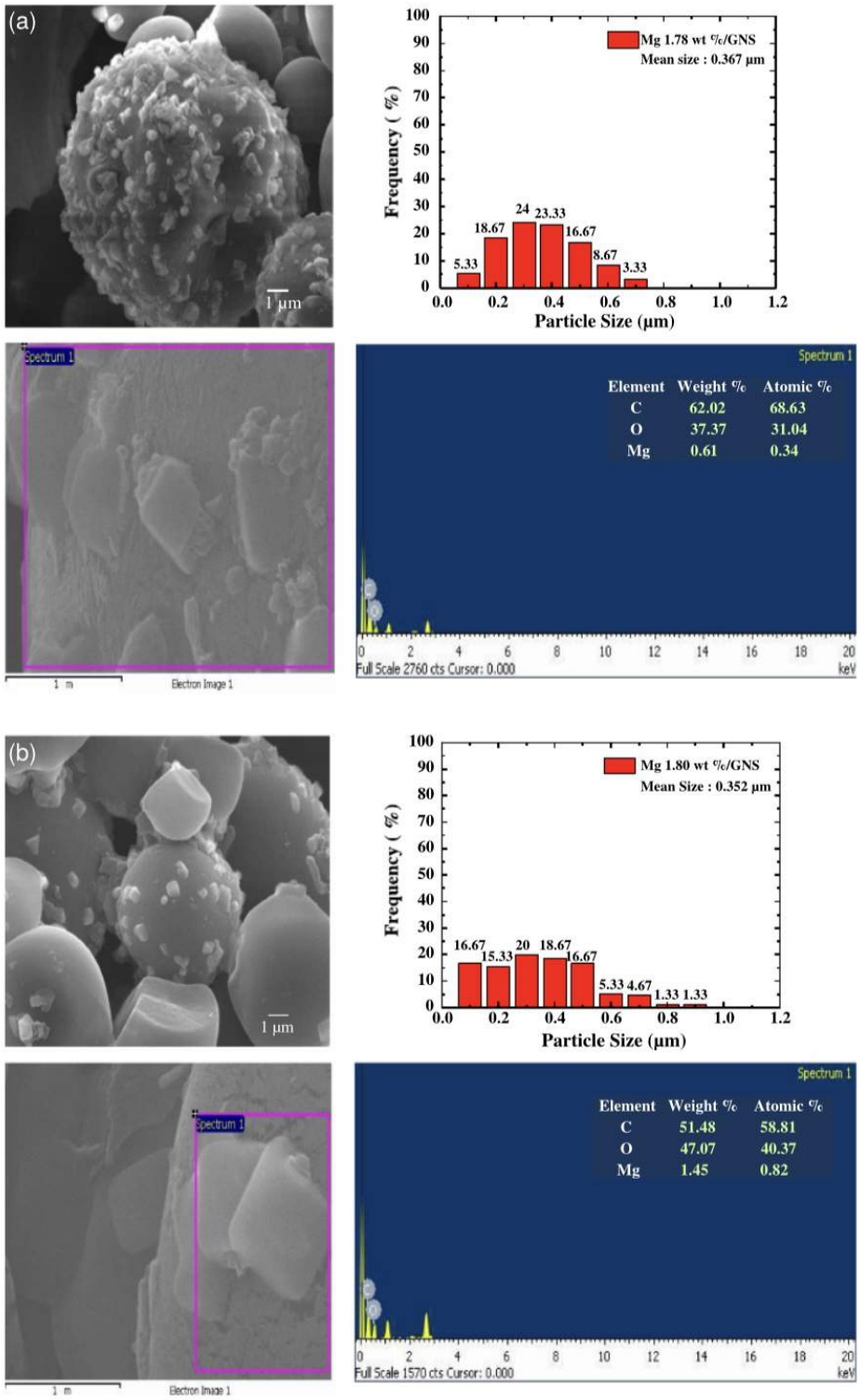

Figure 4. SEM–EDX and particle size histograms of Mg/GNS and Mg/N-GNS with various concentrations of Mg for (a–l) Mg 1.78–2.43 wt%/GNS.

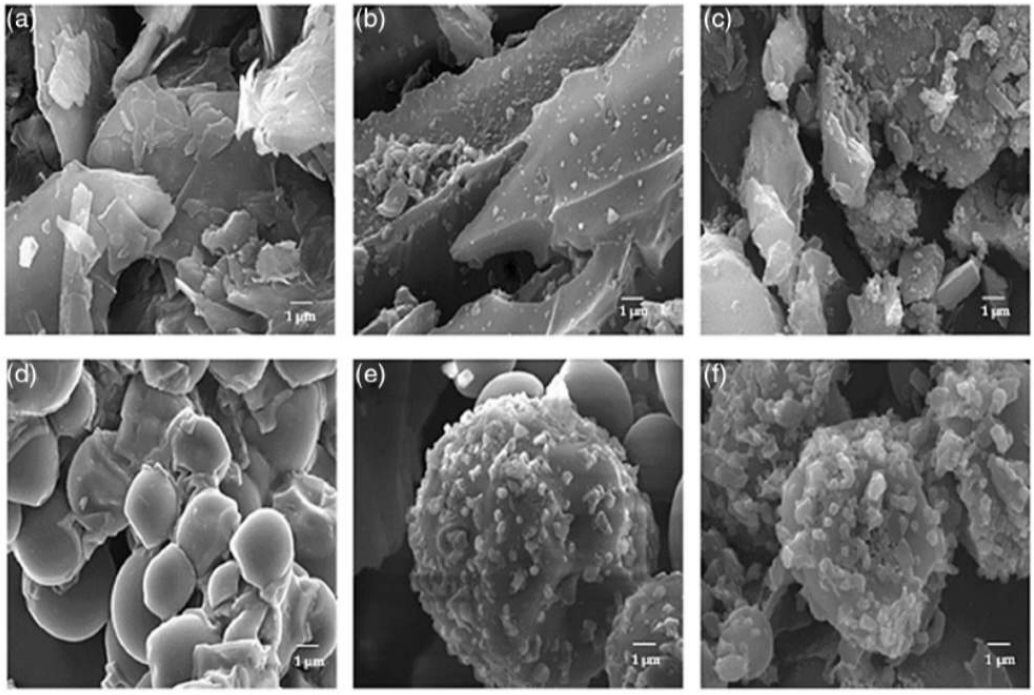

Figure 3. SEM images of a) graphite, b) GNS, c) N-GNS, d) NaCl, e) Mg/GNS, and f) Mg/N-GNS.

from 25 to 30 V. GNS and N-GNS have a maximum electrical conductivity value at 10 V, which then decrease at 15−30 V. This is due to the electron mobility of GNS and N-GNS that increased compared with graphite and is able to produce better electric current, but the three materials cannot easily control the mobility of electrons flowing through the external circuit of an electric current.

From **Figure 7**, it can be seen that the variation in the concentration (wt%) of Mg deposited in the GNS and N-GNS structures (s−π interactions) results in varying current strengths and electrical conductivity of each material. The electrical conductivity values in Mg/GNS and Mg/N-GNS samples depend on the weight concentration and size of the Mg particles that were successfully deposited in the GNS and N-GNS structures. However, based on Figure 7, it can be shown that the samples Mg 1.86 wt%/GNS and Mg 2.43 wt%/N-GNS have the highest electrical conductivity values (63.6945 and 93.4579 $\mu S\ cm^{-1}$) at 30 V. This is due to 1.86 wt%/GNS and Mg 2.43 wt%/N-GNS that have a large/the largest concentration of Mg-deposited mass with relatively smaller particle sizes, evenly distributed on the GNS and N-GNS surfaces compared with Mg/GNS samples with other mass concentrations. These results prove that the addition of Mg metal particles in the GNS and N-GNS structures can increase the electrical conductivity of each material because metal particles can increase the active surface area and the potential for GNS' and N-GNS' ionic diffusion. In addition, Mg metal particles are also able to make GNS and N-GNS have fairly stable electron mobility in releasing electrons. It can be proven that the current generated by each sample tends to increase as the applied voltage increases.

3. Discussion

The research steps begin by dissolving the precursors $MgCl_2.6H_2O$, GNS, and N-GNS with ethanol. Besides functioning to dissolve the precursors, GNS and N-GNS, this step also serves to substitute Cl^- ions from precursors with OH^- ions from ethanol. Next, the Mg−ethanol solution is then mixed with graphene−ethanol and N-graphene−ethanol solution, respectively. This process will cause GNS and N-GNS to reduce Mg^{2+} ions to Mg metal with zero valence and form clusters on the GNS and N-GNS surface. The schematic of all these processes is shown in **Figure 8**. The mechanism of Mg/C-π is shown in Figure 8. The steps consist of the following. 1) The precursor of Mg ($MgCl_2.6H_2O$) was dissolved in ethanol. In this step, the state of precursor Mg (+2) was reduced to be +1. 2) Mg-ion solution was mixed with GNS. The Mg ions were attached on the GNS surface. GNS may donate electrons to Mg ions to form Mg (metal). 3) Mg migrates to the GNS surface to generate Mg particles attached on the GNS surface. Furthermore, the Mg/GNS and Mg/N-GNS material obtained was analyzed by XRD and SEM−EDX.

The Mg/GNS and Mg/N-GNS diffraction patterns displayed a weak and widened peak at $2\theta = 38.5°$ and 44.7°, indicating the peak of magnesium (101) and (102). The 2θ peaks of Mg/GNS and Mg/N-GNS gradually become sharp and narrow with increasing Mg concentrations. This also proves that both GNS and N-GNS succeeded in reducing Mg^{2+} ions from the precursor to zero-valent Mg, and they were deposited in the GNS and N-GNS structures (Figure 2b). Different peak shapes at $2\theta = 38.5$ and 44.7° at various concentrations of Mg/GNS and

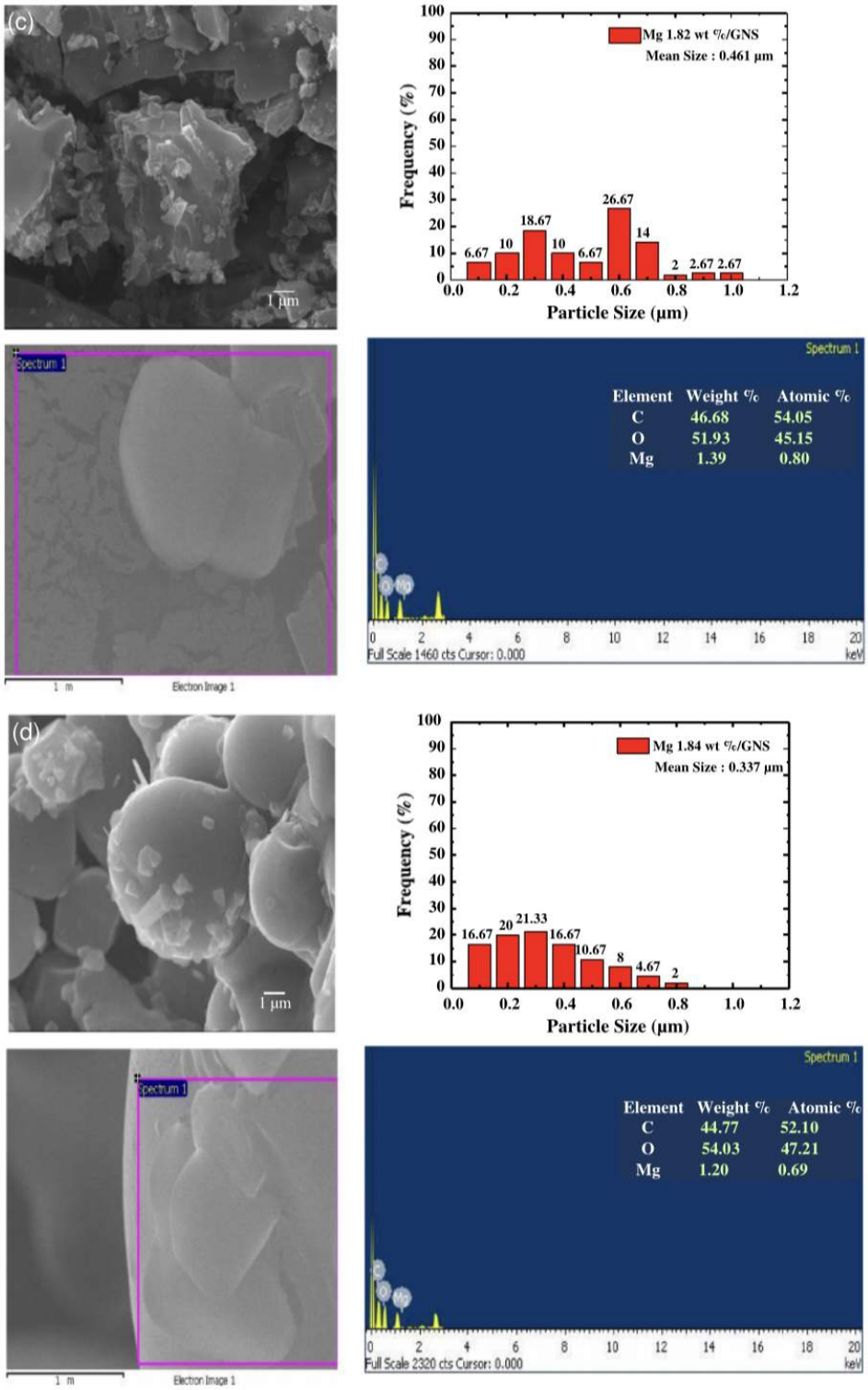

Figure 4. Continued.

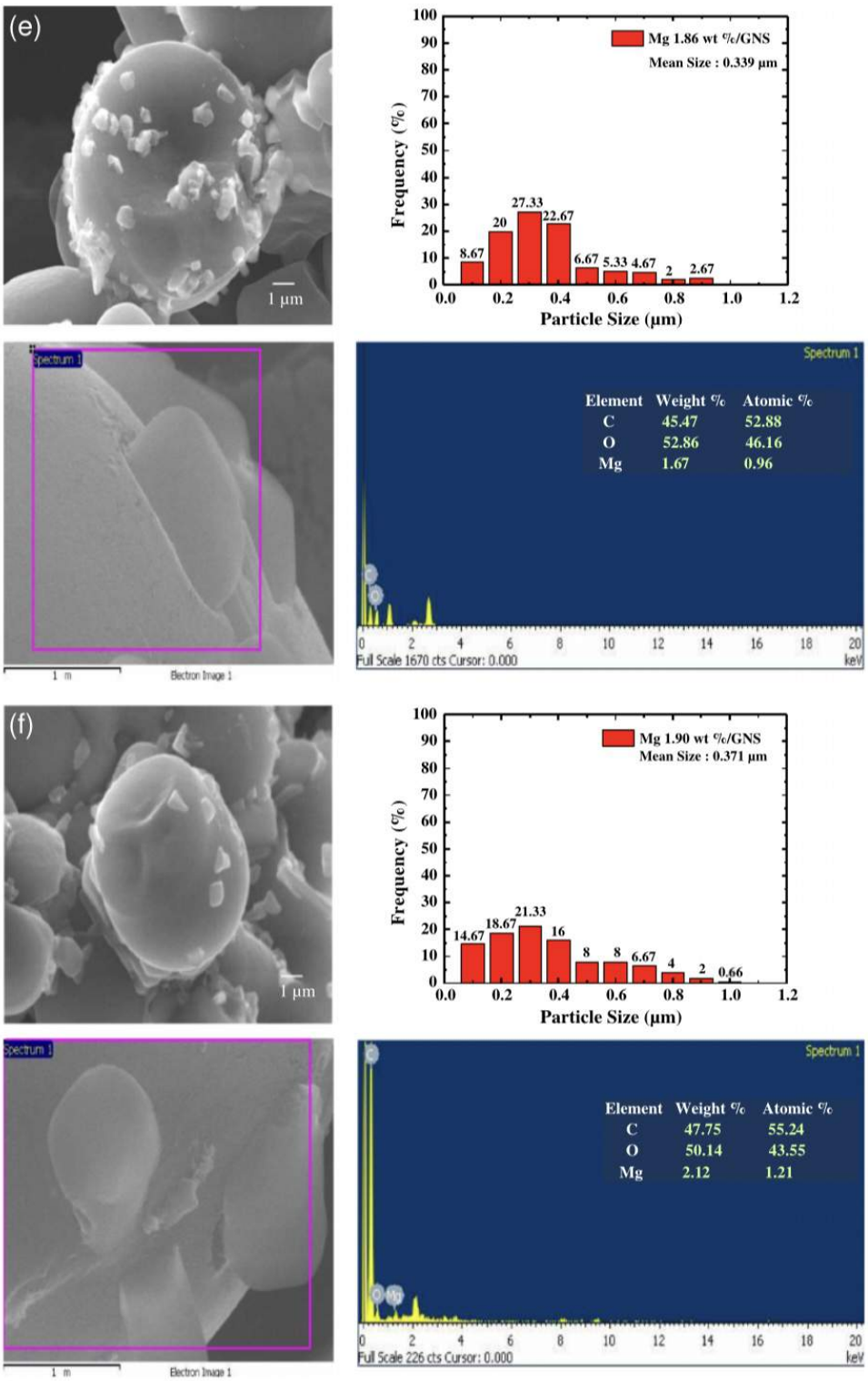

Figure 4. Continued.

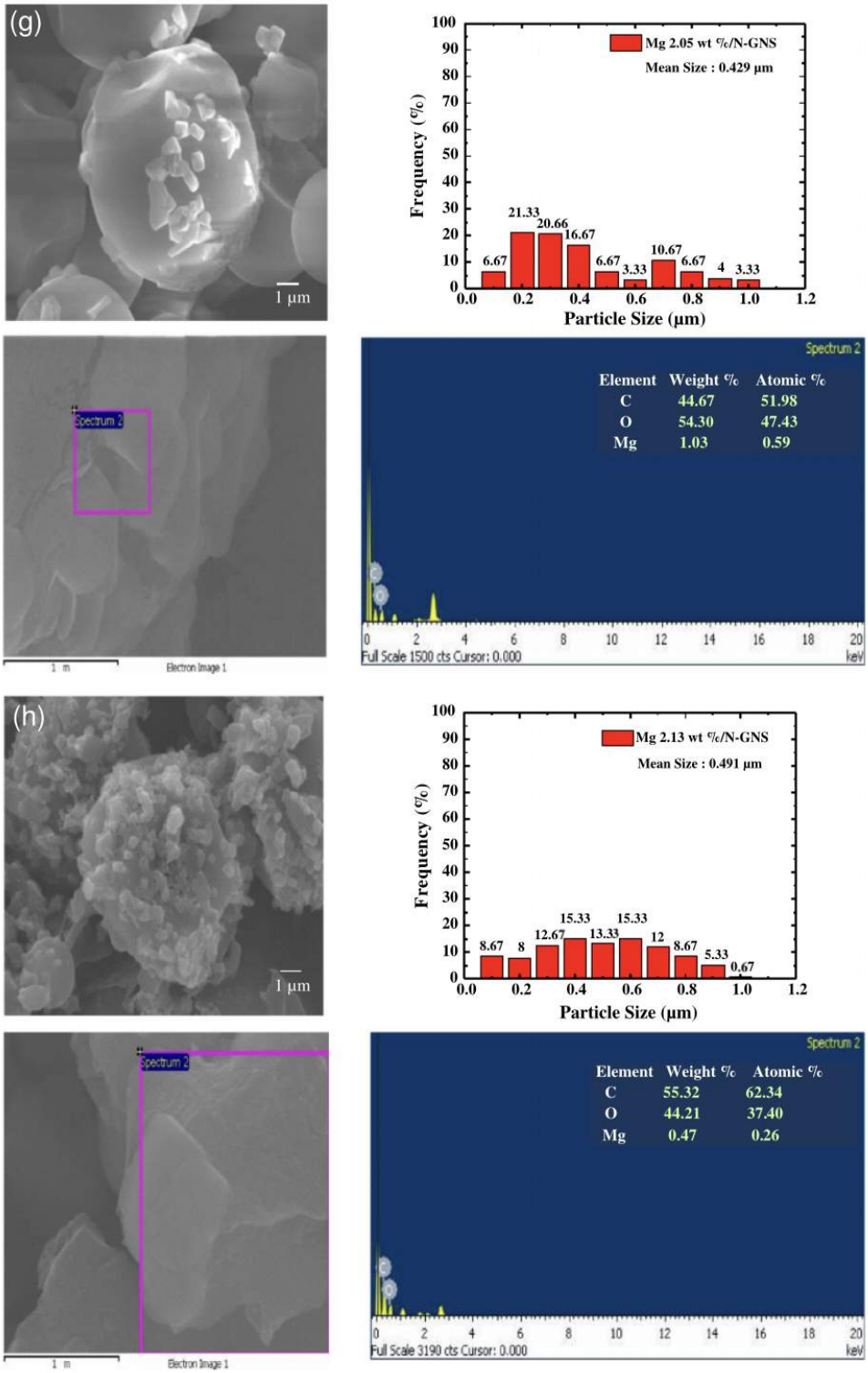

Figure 4. Continued.

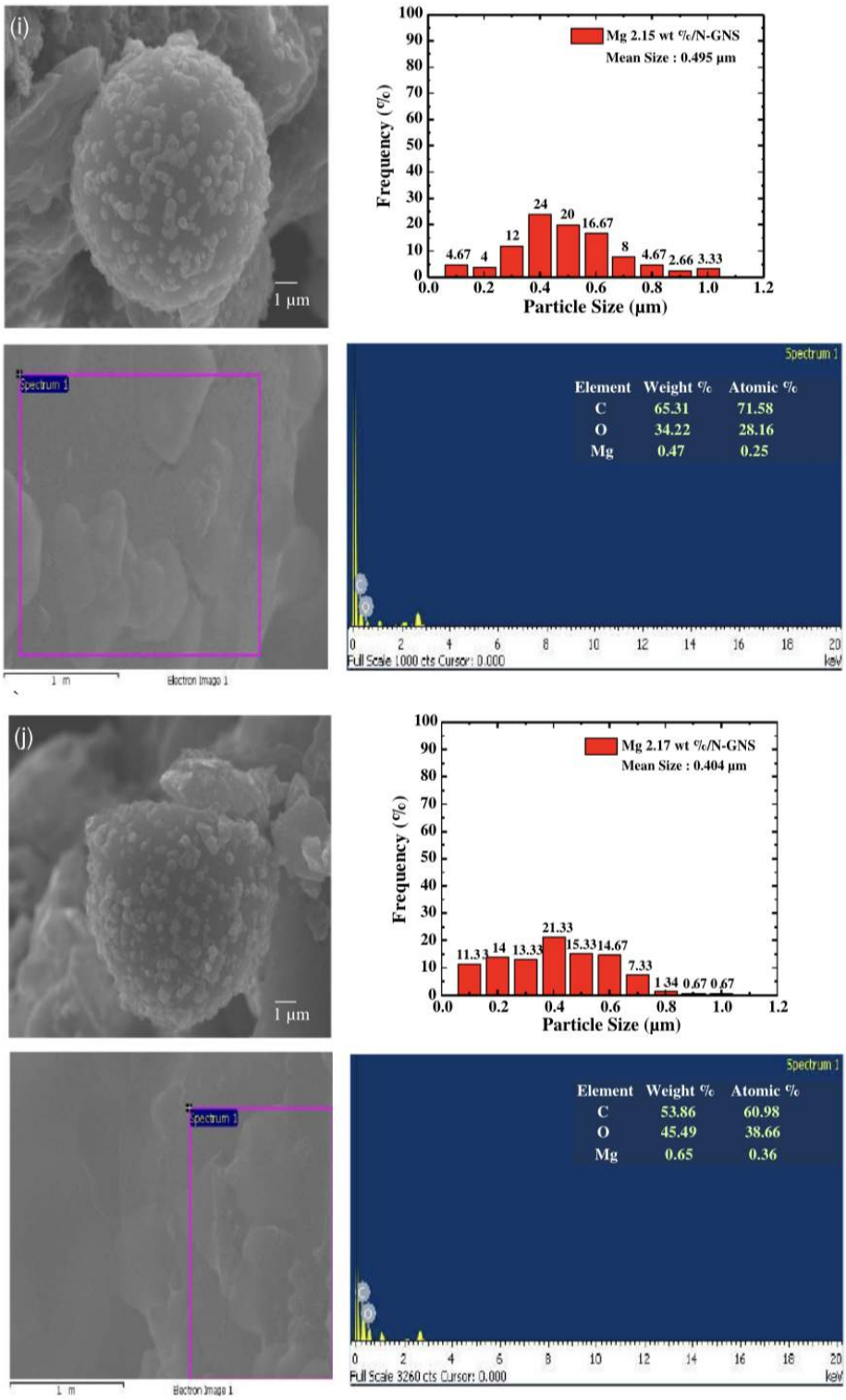

Figure 4. Continued.

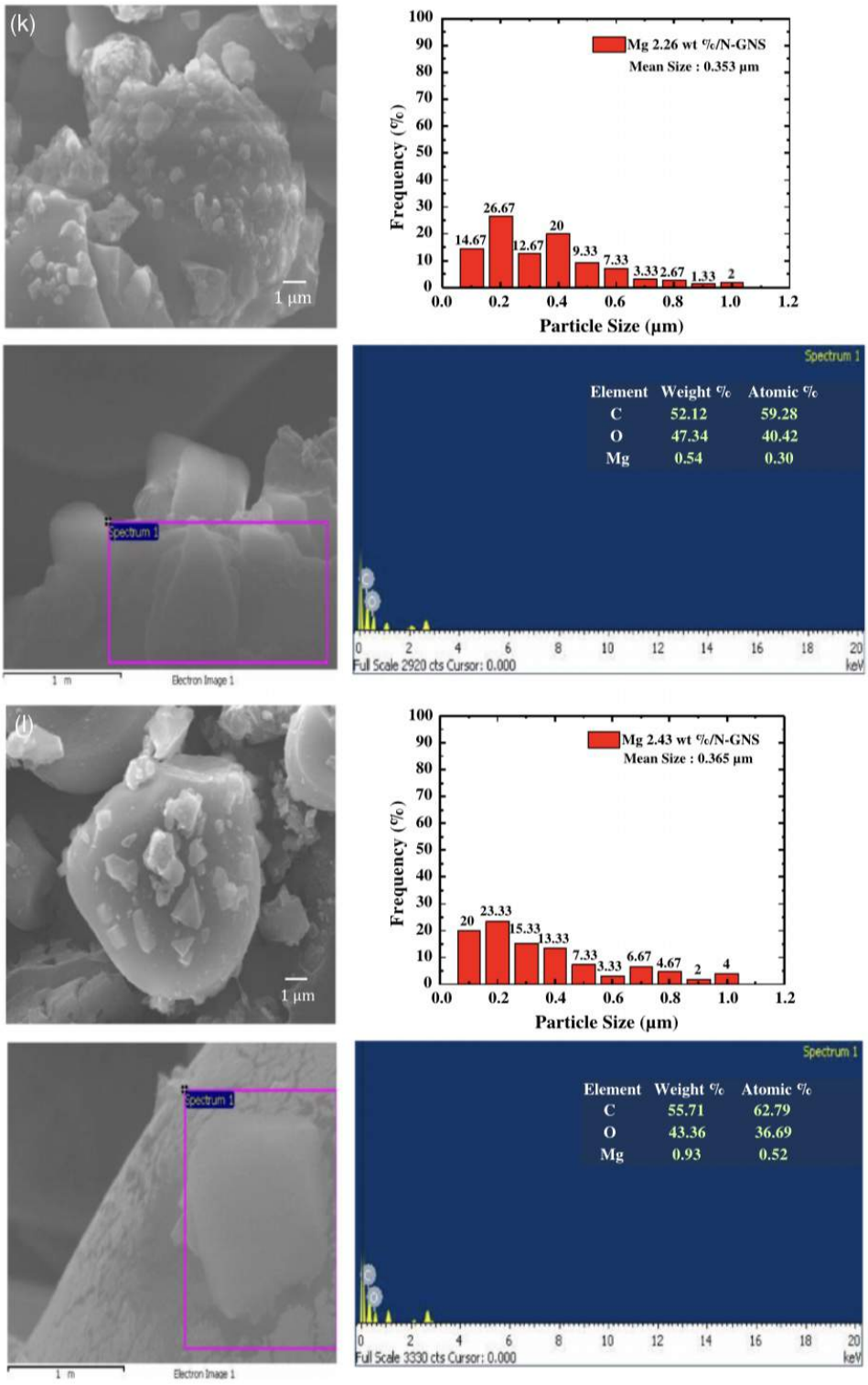

Figure 4. Continued.

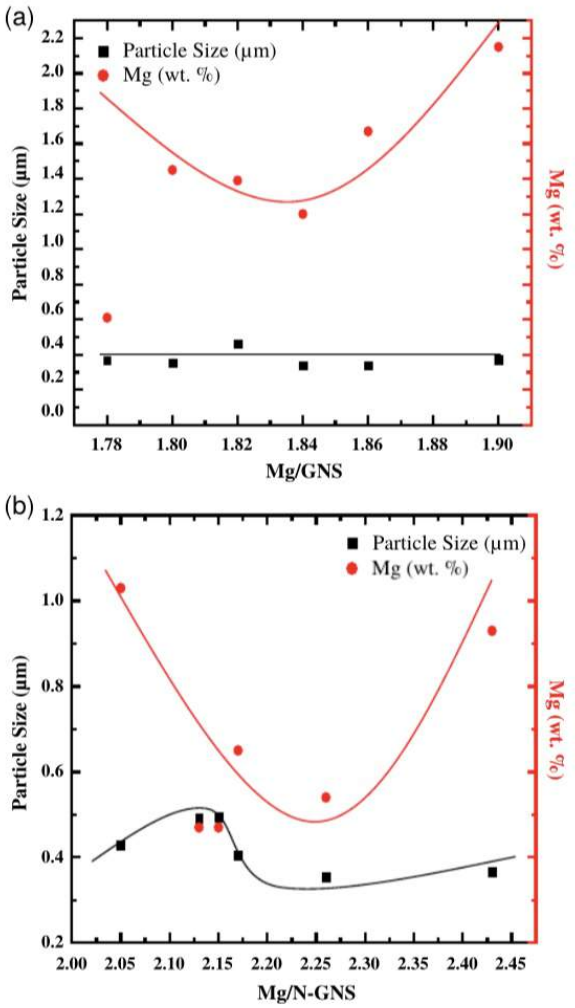

Figure 5. Comparison of the particle size and mass concentration of Mg deposited with the theoretical mass concentration of Mg on a) Mg/GNS and b) Mg/N-GNS.

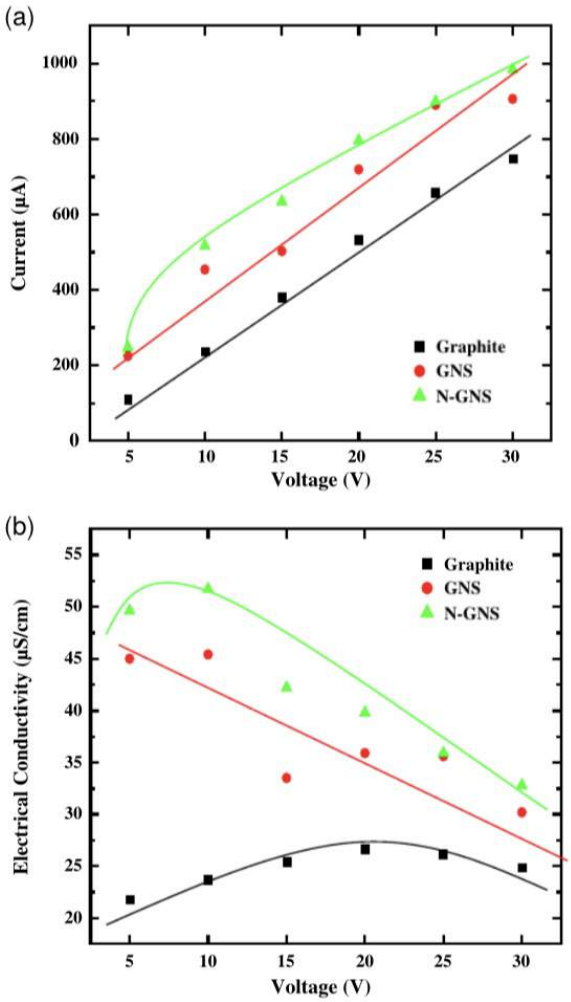

Figure 6. Relation of a) voltage versus current and b) voltage versus electrical conductivity of graphite, GNS, and N-GNS.

interactions between metal block-s (Mg) and π-bond of graphene (s−π bonding). The interaction of magnesium (Mg) with a graphene surface was investigated by the density functional theory (DFT) method. Magnesium atom (Mg) has an electronic configuration of $(3s)^2$ and is one of the *s*-type dopants. The charges of Mg atom on graphene are always negative, indicating that electron transfer occurs from the graphene surface to the Mg atom, in turn indicating that magnesium ion also plays the role of an electron acceptor on the graphene surface. It was found that the Mg atom binds to a hexagonal site of the graphene sheet (Mg atoms bind to the graphene surface).[21]

In graphene, stacked graphene does not so much appear compared with graphite. Graphene consists of thin and smooth layers with an irregular and nonuniform surface (Figure 3b). These data prove that graphene is well formed. N atoms on graphene structures modify graphene. It clearly seems that N-GNS has a uniform surface with a thinner layer than GNS and it has a small pore size and wrinkled surface, which cause the morphology of N-GNS to be different with GNS (Figure 3c). SEM is also used to analyze the morphology of NaCl (as an electrolyte). The surface of NaCl looks like an irregular cube shape (Figure 3d). Figure 3e–f shows Mg/GNS and Mg/N-GNS surfaces, where there are many white spots of various sizes which are uniformly distributed over the GNS and N-GNS surfaces. The morphologies of GNS and N-GNS in Figure 3a,b look different from Mg/GNS and Mg/N-GNS; those are from sheet-like structures to spherical structures. That is possible as Mg particles are deposited on both surfaces of GNS and N-GNS. Interestingly, the Mg particle size on Mg/GNS seems smaller than Mg/N-GNS. In addition, the Mg particles' dispersion is totally different between Mg/GNS and Mg/N-GNS (Figure 3e,f), where the Mg particles are densely dispersed and cover N-GNS surfaces. In contrast, the Mg particles are attached on GNS surfaces, and even the Mg particles are absent at some part of the GNS sheets. Those data

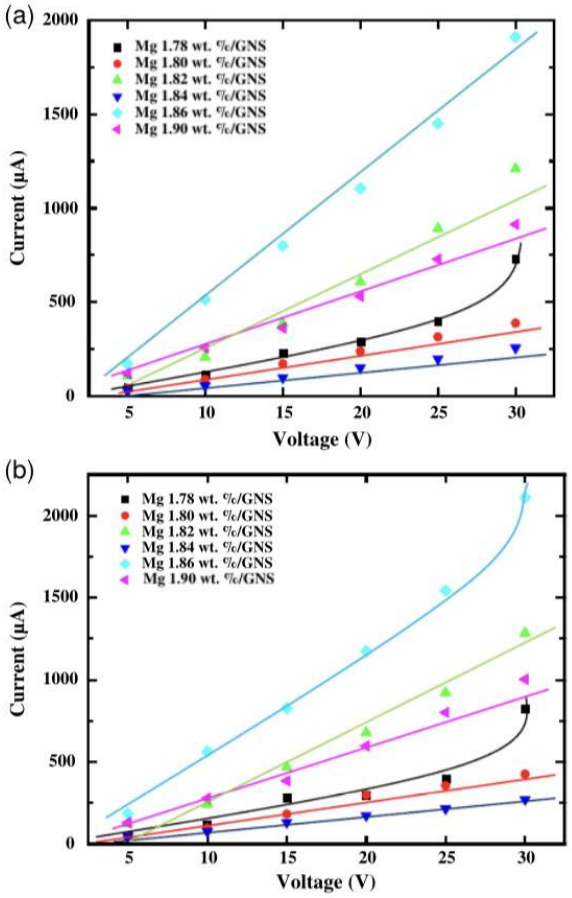

Figure 7. Comparison of voltage versus current of Mg/GNS a) before and b) after adding electrolyte.

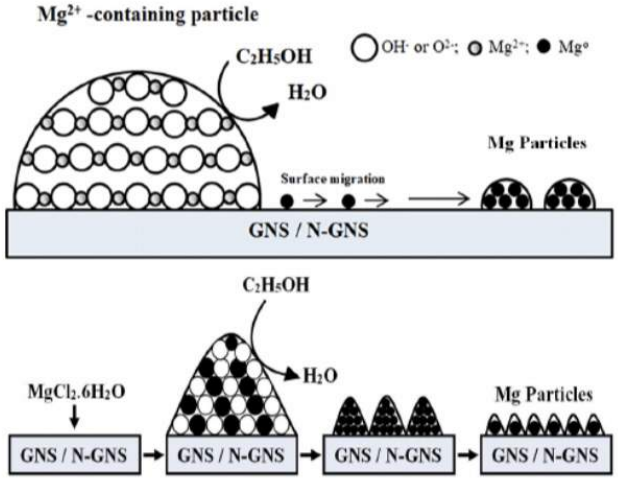

Figure 8. Process of forming Mg subnanocluster.

clearly explain that the size and character of Mg may be affected by GNS and N-GNS.

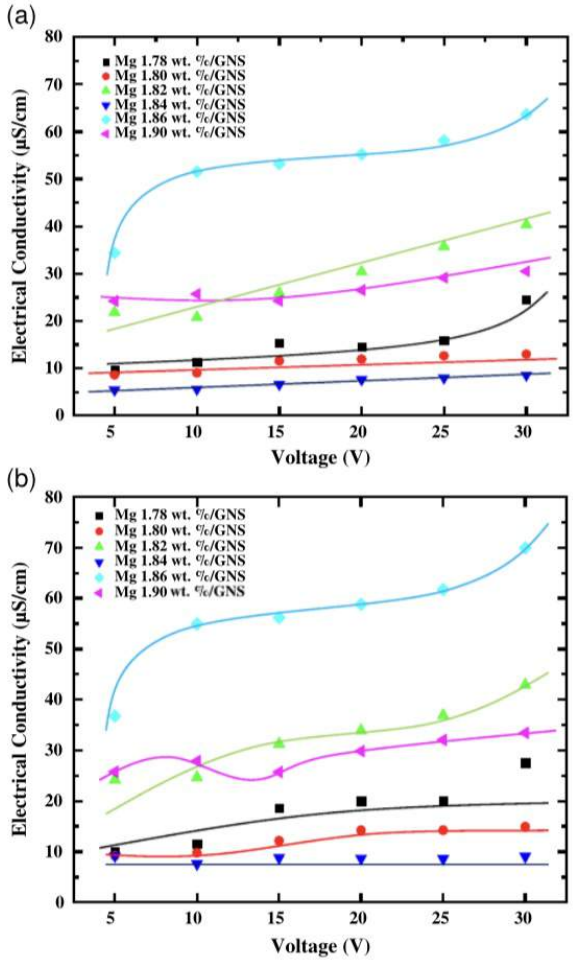

Figure 9. Comparison of voltage versus electrical conductivity of Mg/GNS a) before and b) after adding electrolyte.

The white spots indicate magnesium particles that have been successfully deposited on GNS and N-GNS surface sheets. This further proves that both the GNS and N-GNS structures can manage the size and distribution of metal particles deposited on their surface by the interaction between metal block-s (Mg) and π-bond of graphene (s$-\pi$ bonding). This result is also consistent with our previous work. XRD and EDX data of Mg/graphene show that there is a chemical interaction between Mg and GNS.[44] Mg@graphene binds the complex and partial charge transfer of the higher-energy electrons from graphene to an electron-deficient cation (lowest un-occupied molecular orbital (LUMO) of Mg^{2+} [s-block] and the highest occupied molecular orbital (HOMO) of graphene [π-electron].[45]

Besides depositing Mg metal particles into the GNS and N-GNS structures, the addition of electrolyte also affects the value of the current strength and the electrical conductivity of the sample. **Figure 9–12** shows an increase in electric current and the electrical conductivity of each sample material in the presence of an electrolyte, which is able to regulate and control

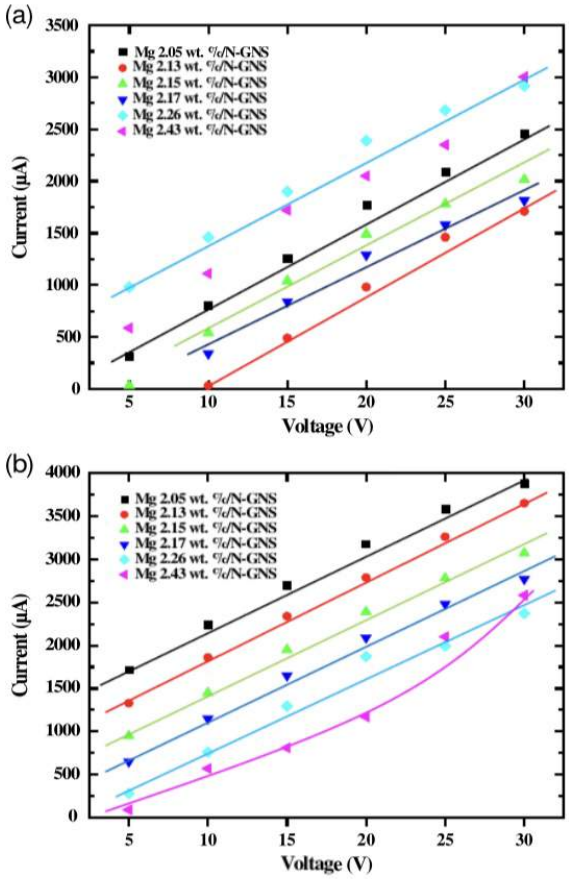

Figure 10. Comparison of voltage versus current of Mg/N-GNS a) before and b) after adding electrolyte.

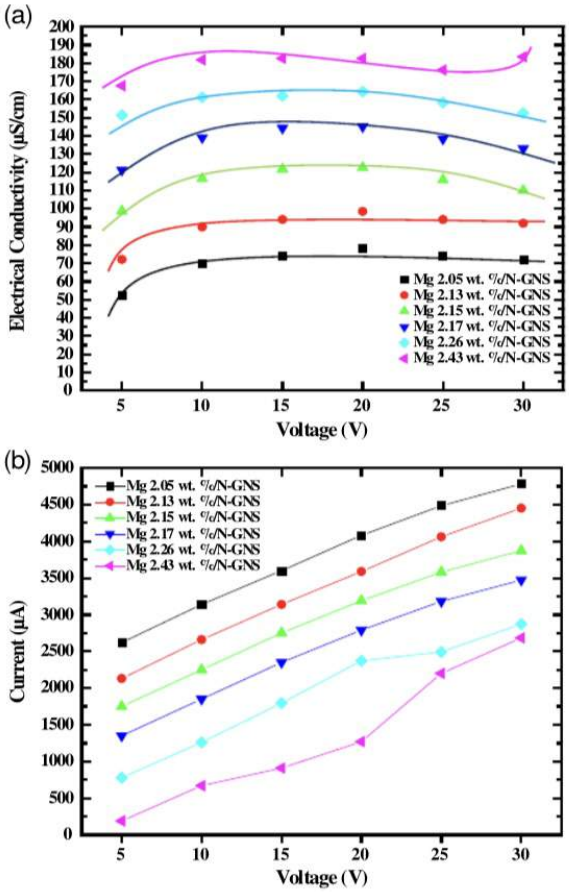

Figure 11. Comparison of voltage versus electrical conductivity of Mg/N-GNS a) before and b) after adding electrolyte.

the rate of electron mobility of each material, so it can increase current strength (≈14.9%) and electrical conductivity (≈12.4%) of Mg/GNS and Mg/N-GNS sample materials. The addition of electrolytes and metal particles in GNS and N-GNS can improve the catalytic, electrical, and electromagnetic properties of both by adjusting the shape of the nanostructures.[39]

To determine the stability of the current strength of Mg 1.86 wt%/GNS and Mg 2.43 wt%/N-GNS, the current strength at the maximum voltage used (30 V) at a time variation of 10−60 min is measured. Based on the measurement data of current strength obtained (Figure 10), it can be shown that Mg 1.86 wt%/GNS and Mg 2.43 wt%/N-GNS materials before and after being combined with NaCl electrolyte experience relatively little electron loss with each added time. This is because Mg has the ability to store electrons in large numbers and can release electrons slowly. However, Mg still has a relatively small reducing power. With the addition of the electrolyte NaCl to Mg/GNS and Mg/N-GNS, it is able to increase the reducing power of Mg by controlling the mobility of the electrons flowing through its structure, which allows the rate of energy consumption to be slightly longer.

4. Conclusion

The method of preparing Mg/GNS and Mg/N-GNS can be conducted by the impregnation method, in which Mg metal is successfully obtained through the process of reducing Mg^{2+} ions from the precursor $MgCl_2.6H_2O$ to Mg with zero valence by the surface structure of GNS and N-GNS and deposited well above their surface. Although the concentration of the Mg precursor used varies, GNS and N-GNS are able to control the size and distribution of the metal particles that interact or are deposited into their structures. The interaction that occurs between Mg metals with the GNS and N-GNS structures (s−π interaction) can increase the value of the current and electrical conductivity of GNS and N-GNS because Mg metal particles have the ability to store electrons in large numbers and can release electrons slowly. In addition, Mg metal particles can also open the energy gap between the GNS and N-GNS conductance and valence bands, so as to increase the active surface area, electron mobility, and the ionic diffusion potential of GNS and N-GNS. The addition of electrolyte is also known to be able to increase the value of current and electrical conductivity due to the basic nature of electrolytes, which easily conduct electric current, increase the

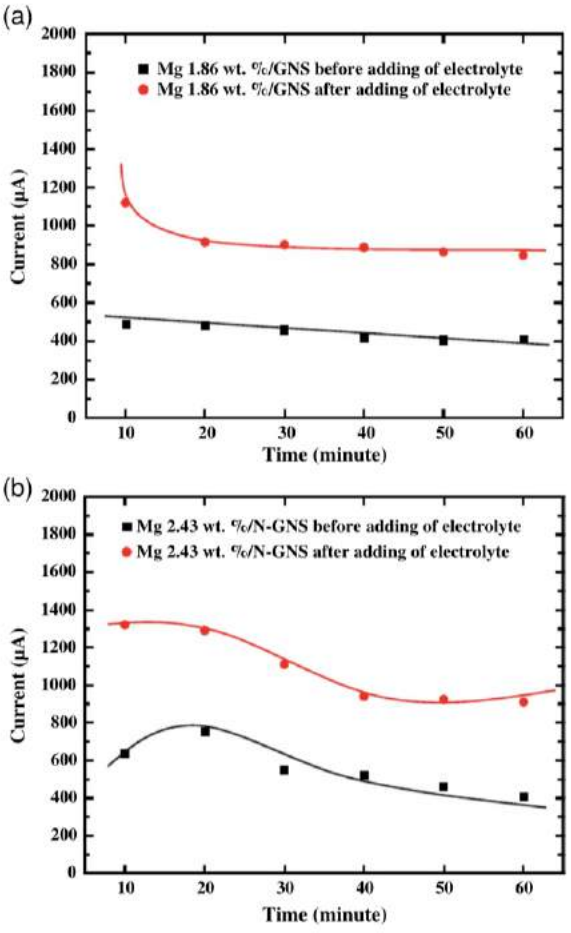

Figure 12. Comparison of the time and current relationship of Mg 1.86 wt%/GNS and Mg 2.43 wt%/N-GNS with the conditions before and after electrolyte addition.

reduction power of Mg metal particles, and control the mobility of electrons through the structure of each sample material.

5. Experimental Section

Chemicals: Graphite commercial powder (carbon 98 wt% and ash 15 wt%), potassium permanganate ($KMnO_4$, 99 wt%), hydrogen peroxide (H_2O_2, 30 wt%), sulfuric acid (H_2SO_4, 98 wt%), and ammonia (NH_3, 25 wt %) were obtained from Sigma-Aldrich (Singapore). Sodium nitrate ($NaNO_3$, 99 wt%), sodium chloride (NaCl, 99 wt%), and magnesium chloride hexahydrate ($MgCl_2.6H_2O$, 99 wt%) were purchased from Merck (Singapore). All the chemical reagents were used as approved without any further purification.

Synthesis of GNS: First of all, graphite was oxidized to produce graphene oxide (Hummers and Offenman's method).[40] Briefly, 0.2 g of graphite was mixed with 0.2 g $NaNO_3$ and 15 mL H_2SO_4 then, graphite solution was stirred for 1 h in an ice bath condition. After 1 h, 1 g $KMnO_4$ was gradually added into the graphite solution and stirred for 24 h. Subsequently, graphite solution was added to 20 mL of H_2SO_4, 5%, and 1 mL H_2O_2, 30%, and stirred for 1 h, respectively, to produce graphite oxide. Then, graphite oxide was centrifuged at 6500 rpm for 20 min in piranha solution and ultrasonicated for 6 h, producing a solution of graphene oxide. The solution of graphene oxide then was reduced using 5 mL NH_3 10 M and it was stirred for 72 h, filtered, and dried at 100 °C to produce graphene powder.[41,46]

Synthesis of N-GNS: Graphene powder then was reduced using 5 mL NH_3 10 M and it was stirred for 72 h. Then, the solution was filtered and dried at 100 °C to produce N-graphene powder.[47]

Preparation of Mg Standard Solution: The Mg standard solutions (100 and 10 mg L^{-1}) were prepared by diluting 10 mL of Mg solution with concentrations of 1000 and 100 ppm in a 100 mL measuring flask with distilled water, respectively. Then, to make standard solutions of Mg 1, 2, 3, 4, and 5 mg L^{-1}, we diluted 10, 20, 30, 40, and 50 mL of standard 10 mg L^{-1} Mg solution in 100 mL measuring flasks with distilled water, respectively.

Preparation of Mg/GNS and Mg/N-GNS: 0.5 g of graphene powder was put in a beaker glass, which contained a standard series solution of 1 ppm magnesium, and was stirred for 2 h to produce a magnesium–graphene mixture. The magnesium–graphene mixture was filtered with Whatman filter paper no. 42 and the filtrate was produced and precipitated. The precipitate obtained was dried at 80 °C for 2 h. A solid powder was produced and labeled as Mg 1 mg/L/GNS. The same procedure was conducted to prepare 2, 3, 4, 5, and 10 Mg mg/L/GNS. The resulting Mg/GNS powder was then weighed to calculate the approximate mass and concentration of Mg that was successfully deposited on the GNS/N-GNS structure theoretically.[44]

Electrolyte Paste Preparation: As much as 10 g of sodium chloride (NaCl) was mixed with 2 g of starch, little distilled water was added, and then it was homogenized to form a paste. The electrolyte that was prepared was combined with Mg/GNS and Mg/N-GNS powder and then tested for their electrical conductivities.[44]

Materials Characterization: Graphite, GNS, N-GNS, Mg/GNS, and Mg/N-GNS were characterized by XRD and SEM–EDX. X-ray diffraction measurements were carried out at room temperature using X-ray Rigaku Smartlab 3 kW with Cu Kα radiation (1.540598α), scanning speed of 2° min^{-1}, voltage 44 kV, and current 40 mA to observe samples from 5° to 80° of 2θ (degree). SEM–EDX analysis used EM 30 COXEM with a voltage of 20 000 kV with enlargement of 100–4000 times.

Electrical Conductivity Measurement: Graphite powder was put into the fuse tube, compacted, and covered with a fuse cover. It was connected the positive and negative poles of the fuse with multimeter CD800A Sanwa and Regulated DC Power Supply (ATTEN) using an alligator clamp cable. Electrical conductivity was measured at various voltages of 5, 10, 15, 20, 25, and 30 V. The current measurement result (μA) was recorded, which was displayed on the multimeter. The same measurement steps were conducted for GNS, N-GNS, Mg/GNS, Mg/N-GNS powders, and the alloys of each material with NaCl electrolyte paste with a ratio of 1:1.

Acknowledgements

We would like to thank DRPM, Kemendikbud-Ristek who supported this research under scheme Skema Penelitian Dasar, No. 100/UN5.2.3.1/PAP/KP-DRPM/2021. Hardy Shuwanto, Roy Simanjuntak, PT Lab Sistematika Indonesia and PT Gestrindo-Jakarta who also have supported the author on XRD, SEM-EDX analysis and electrical conductivity test of samples.

Conflict of Interest

The authors declare no conflict of interest.

Data Availability Statement

Research data are not shared.

Keywords

electrical conductivity, graphene, graphite, Mg/GNS, Mg/N-GNS, NaCl, N-graphene

Received: May 27, 2021
Revised: August 1, 2021
Published online:

[1] G. Jeong, Y. U. Kim, H. Kim, Y. J. Kim, H. J. Sohn, *Energy Environ. Sci.* **2011**, *4*, 1986.
[2] H. K. Yee, S. Ramakrishnan, A. A. Mohamad, *J. Quality Meas. Anal.* **2014**, *10*, 39.
[3] J. Hou, Y. Shao, M. W. Ellis, R. B. Moore, B. Yi, *Phys. Chem. Chem. Phys.* **2011**, *13*, 15384.
[4] M. J. Allen, V. C. Tung, R. B. Kaner, *Chem. Rev.* **2010**, *110*, 132.
[5] K. Liu, Y. Liu, D. Lin, A. Pei, Y. Cui, *Sci. Adv.* **2018**, *4*, 9820.
[6] G. J. May, A. Davidson, B. Monahov, *J of Energy Storage* **2017**, *15*, 145.
[7] Y. Si, E. T. Samulski, *Nano Lett.* **2008**, *8*, 1679.
[8] C. C. Chang, Y. C. Lee, H. J. Liao, Y. T. Kao, J. Y. An, D. Y. Wang, *ACS Sustainable Chem. Eng.* **2019**, *7*, 860.
[9] G. Lombardo, B. Ebin, M. R. St. J. Foreman, B. M. Steenari, M. Petranikova, *ACS Sustainable Chem. Eng.* **2019**, *7*, 13668.
[10] G. E. Blomgren, *J. Electrochem. Soc.* **2017**, *164*, A5019.
[11] F. Wang, X. Wu, C. Li, Y. Zhu, L. Fu, Y. Wu, X. Liu, *Energy Environ. Sci.* **2016**, *9*, 3570.
[12] M. K. Loganathan, C. M. Tan, B. Mishra, T. A. M. Msagati, L. W. Snyman, *IEEE Transp. Electr. Conf. (ITEC–India)* **2019**, *254*, 19575819.
[13] J. S. Lee, G. S. Park, H. I. Lee, S. T. Kim, R. Cao, M. Liu, J. Cho, *Nano Lett.* **2011**, *12*, 5362.
[14] N. Xue, W. Du, J. R. R. A. Martins, W. Shyy, *Handbook of Clean Energy Systems, Energy Storage*, 5 ed., John Wiley and Sons, Ltd, Chichester **2015**.
[15] L. Xia, S. Wang, G. Liu, L. Ding, D. Li, H. Wang, S. Qiao, *Small* **2016**, *12*, 853.
[16] L. Lavagna, G. Meligrana, C. Gerbaldi, A. Tagliaferro, M. Bartoli, *Energies* **2020**, *13*, 4867.
[17] N. Loeffler, D. Bresser, S. Passerini, *Johnson Matthey Technol. Rev.* **2015**, *59*, 34.
[18] X. Meng, *IOP Conf. Ser.: Earth Environ. Sci.* **2019**, *300*, 042039.
[19] X. Liu, C. Z. Wang, M. Hupalo, H. Q. Lin, K. M. Ho, M. C. Tringides, *Crystals* **2013**, *3*, 79.
[20] S. Wang, B. Yang, H. Chen, E. Ruckenstein, *J. Mater. Chem. A* **2018**, *6*, 6815.
[21] H. Tachikawa, T. Iyama, H. Kawabata, *Thin Solid Films* **2009**, *518*, 877.
[22] L. Li, S. Li, T. Zeng, L. Deng, H. Huang, J. Li, N. Kobayshi, L. Liu, Y. Zhou, *Energy Technol.* **2021**, *9*, 2170073.
[23] Q. Guo, W. Zeng, S. L. Liu, Y. Q. Li, J. Y. Xu, J. X. Wang, Y. Wang, *Rare Met.* **2020**, *40*, 290.
[24] M. R. Al. Hassan, A. Sen, T. Zaman, M. S. Mostari, *Mater. Today Chem.* **2019**, *11*, 225.
[25] A. Jana, D. R. Ely, R. E. García, *J. Power Sources* **2015**, *275*, 912.
[26] S. M. Choi, M. H. Seo, H. J. Kim, W. B. Kim, *Synth. Met.* **2011**, *161*, 2405.
[27] M. Terrones, A. R. Botello-Méndez, J. Campos-Delgado, F. López-Urías, Y. I. Vega-Cantú, F. Rodríguez-Macías, J. C. Charlier, *Nano Today* **2010**, *5*, 351.
[28] A. Sinha, A. Sharma, A. Priyadarshi, B. M. Tulapurkar, *Phys. Rev. Mater.* **2019**, *3*, 124005.
[29] L. Malyala, S. Thatipamula, V. R. Jetti, *Trans. Indian Inst. Met.* **2019**, *72*, 2503.
[30] W. Qi, J. G. Shapter, Q. Wu, T. Yin, G. Gao, D. Cui, *J. Mater. Chem. A* **2017**, *5*, 19521.
[31] Y. Orikasa, T. Masese, Y. Koyama, T. Mori, M. Hattori, K. Yamamoto, T. Okado, Z. D. Huang, T. Minato, C. Tassel, J. Kim, Y. Kobayashi, T. Abe, H. Kageyama, Y. Uchimoto, *Sci. Rep.* **2014**, *4*, 5622.
[32] M. Walter, M. V. Kovalenko, K. V. Kravchyk, *New J. Chem.* **2020**, *44*, 1677.
[33] X. Liu, C. Z. Wang, M. Hupalo, W. C. Lu, M. C. Tringides, Y. X. Yao, K. M. Ho, *Phys. Chem. Chem. Phys.* **2012**, *14*, 9157.
[34] G. Zhao, X. Li, M. Huang, Z. Zhen, Y. Zhong, Q. Chen, X. Zhao, Y. He, R. Hu, T. Yang, R. Zhang, C. Li, J. Kong, J. B. Xu, R. S. Ruoff, H. Zhu, *Chem. Soc. Rev.* **2017**, *46*, 4417.
[35] T. C. Mendes, X. Zhang, Y. Wu, P. C. Howlett, M. Forsyth, D. R. Macfarlane, *ACS Sustainable Chem. Eng.* **2019**, *7*, 3722.
[36] Y. Li, H. Junyan, L. Gang, L. Hongtao, *Chem. Eng. J.* **2014**, *258*, 320.
[37] N. Chalmpes, K. Spyrou, A. B. Bourlinos, D. Moschovas, A. Avgeropoulos, M. A. Karakassides, D. Gournis, *Molecules* **2020**, *25*, 297.
[38] A. N. Popova, *Coke Chem.* **2017**, *60*, 361.
[39] K. Karuppanana, A. V. Raghu, M. K. Panthalingal, V. Thiruvenkatam, P. Karthikeyan,Pullithadathil, *Sustainable Energy Fuels* **2019**, *3*, 996.
[40] H. S. Hummers, R. E. Offeman, *J. Am. Chem. Soc.* **1958**, *80*, 1339.
[41] R. Siburian, J. Nakamura, *J. Phys. Chem. C.* **2012**, *116*, 22947.
[42] X. M. Du, K. F. Zhen, F. G. Liu, *Dig. J. Nanomater. Biostruct.* **2018**, *13*, 827.
[43] Y. Shang, H. Xu, M. Li, G. Zhang, *Nano* **2017**, *12*, 1750018.
[44] C. Simanjuntak, R. Siburian, H. Marpaung, Tamrin, *Heliyon* **2020**, *6*, 03118.
[45] G. Colherinhas, E. E. Fileti, V. V. Chaban, *J. Phys. Chem. Lett.* **2015**, *6*, 302.
[46] R. Siburian, H. Sihotang, S. Lumban Raja, M. Supeno, C. Simanjuntak, *Orient. J. Chem.* **2018**, *34*, 182.
[47] R. Siburian, Dewiratih, Andiayani, S. Perangin-angin, H. Sembiring, H. Sihotang, S. Lumbanraja, M. Supeno, N. Pasaribu, C. Simanjuntak, S. P. Aritonang, *Orient. J. Chem.* **2018**, *34*, 1978.